IEEE Robotics and Automation Letters (RA-L) paper, presented at ICRA 2026, Vienna, Austria. Cite as RA-L paper.

# How to Shake Trees With Aerial Manipulators? A Theoretical and Experimental Study

Antonio González-Morgado, Eugenio Cuniato, Guillermo Heredia, Aníbal Ollero, Roland Siegwart, Marco Tognon

***Abstract*— Aerial manipulators are advancing beyond traditional inspection roles to enable complex interactions with flexible structures. Applications such as structural health monitoring, and especially agricultural tasks like fruit harvesting or environmental monitoring, require inducing controlled vibrations into flexible elements. However, current solutions for controlled shaking of trees with aerial manipulators are limited to push and pull forces applied through translational movements, without exploiting the fully-capabilities of aerial platforms. This paper introduces a controlled shaking strategy that enables interaction with trees using both linear movements generated by forces (*translation strategy*) and rotational movements generated by torques (*rotation strategy*) thus exploiting the different interaction capabilities of the platform. These two strategies open a previously unexplored question: which strategy is more effective given a specific interaction point? To address this, the two interaction strategies are integrated with the Rayligh-Ritz model of the tree, obtaining the closed-loop dynamics of the system during the vibration. These closed-loop dynamics are then analyzed for the two shaking strategies, deriving which one is better for achieving higher oscillation amplitudes or frequencies. This analysis shows that, for a given interaction point of the tree trunk, this decision depends only on the platform's physical characteristics, such as mass and inertia. Finally, the theoretical analysis is experimentally validated with a hand-made bamboo tree and a fully-actuated platform through indoors flights.**

## I. INTRODUCTION

In recent years, aerial manipulators [1] have expanded their range of tasks from the inspection of oil and gas refineries [2] to direct interaction with flexible elements [3]. However, new tasks, such as canopy sampling [4], introduce additional challenges arising from the interaction between the aerial platform and deformable structures.

In the field of agriculture and environmental science, aerial manipulators offer unique advantages. Compared to ground-based robots, aerial manipulators can access hard-to-reach areas and operate over uneven terrains commonly found in mountainous or forested environments. In addition, they can reach high-altitude branches and fruits that are often inaccessible or inefficient to harvest using ground robots. Therefore, aerial manipulators present a promising solution for tasks such as fruit harvesting, canopy sampling, or precision agriculture operations in complex natural environments.

Beyond physical access, several agricultural applications specifically require the ability to induce vibrations in trees or branches. An example is the shake-and-catch method [5], one of the most used techniques for mechanical fruit harvesting. In this approach, vibrations are introduced into the tree by a mechanical shaker [6], which generates sufficient force to detach the fruit by breaking the stem-fruit interface. Similarly, tree vibration is also essential for structural health monitoring and the estimation of biomechanical parameters. Methods used to identify properties (natural frequency, damping ratio, or stiffness) require excitation of the tree [7]. These parameters are indicators of a tree's condition and can reveal structural damage or degradation over time when changes are detected [8]. However, both harvesting and monitoring tasks currently rely on ground-based shakers, often requiring human presence, which limits scalability and access in difficult terrain. In this context, aerial manipulators offer an alternative for enabling shaking tasks in hard-to-reach areas and in a remote way. In addition, their use as shaking tools enables novel applications, such as environmental DNA (eDNA) sampling [9], where the aerial robot shakes branches to release biological material that can then be collected by ground robots.

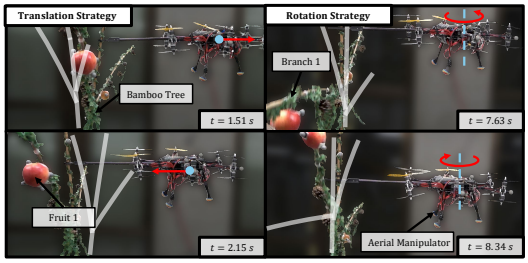


Fig. 1. Aerial manipulator shaking a tree. Left: shaking with translations. Right: shaking with yaw rotations. The white lines represent the tree at the previous time instant, illustrating the deformation over time, while the red arrows shows the taken control actions to shake de tree.

In particular, in our last work [10] we presented a control framework for shaking trees with aerial manipulators. The proposed shaking controller interacts with the tree through pull and push forces generated by translational movement, achieving oscillations at the system's natural frequency. Additionally, we developed a tree model based on the Rayleigh-Ritz method. By combining this model with the proposed controller, we obtained the vibration frequency and amplitude of the UAV-tree system, which depend on the interaction point and the mass of the platform. Based on this analysis, we identified optimal interaction points on the tree trunk to achieve either high oscillation frequencies or

A. Gonzalez-Morgado (corresponding author: mantonio@us.es.), G. Heredia and A. Ollero are with the GRVC Robotics Lab, Sevilla, Spain. E. Cuniato, and R. Siegwart are with the Autonomous Systems Lab (ASL), ETH Zurich. M. Tognon is with Univ Rennes, Inria, Rennes, France.

large oscillation amplitudes.

However, the shaking controller presented in that work is limited to interactions through displacements along one direction only, without exploiting other types of interaction that a fully-actuated platform could offer. Since the strategy is restricted to translational movements, the mass of the UAV influences the closed-loop oscillation amplitudes and frequencies. For other types of movements, the UAV could differently influence the closed-loop behavior. For example, if the UAV interacts through rotational movements, its rotational inertia would affect the closed-loop behavior instead of its mass. However, in that study, the oscillation strategy was fixed and not a decision variable. Consequently, the analysis performed was limited to selecting the interaction point on the tree trunk without considering in this decision the different actuation capabilities that the aerial platform can offer.

### A. Contributions and Novelties

In this work, we take into account the characteristics of the aerial platform, such as mass and inertia, to inform the selection of the shaking strategy. The approach in our previous work focused on selecting the interaction point on the tree trunk for the shaking task, assuming that the platform could access all points on the trunk. However, in real trees, which are full of branches, only one or a few points on the trunk are accessible, and therefore, it is sometimes not possible to choose the interaction point. The approach in this work focuses on selecting the interaction strategy with the tree, given a specific interaction point. The two interaction strategies are translation strategy and the rotation strategy. While the translation strategy excites the tree through linear movements of the aerial robot that generate pull-and-push forces at the contact point, the rotation strategy induces oscillations by applying torque through yaw rotations of the aerial robot. In summary, this work addresses the following question: *For a given interaction point on the tree trunk, is it better to interact through the translation strategy or the rotation strategy?* This decision is important because each strategy leads to different closed-loop dynamics. In the translation strategy, the UAV's mass influences the system behavior, whereas in the rotation strategy, its rotational inertia becomes dominant. These differences affect the oscillation amplitude and frequency of the tree achieved during the closed-loop interaction, directly impacting the effectiveness of the shaking process. Although the approach of this work can be applied to the controlled shaking of any flexible system, in this work we focus on tree shaking as a representative application, particularly relevant in agricultural and environmental tasks.

To do so, we extend the shaking controller to interact with different types of movements, not just through translational displacements achieved by the translation strategy (see Fig. 1-left). Specifically, we expand the controller to interact through yaw rotations using a rotation strategy, as shown in Fig. 1-right. This new type of interaction modifies the achieved closed-loop oscillations, as the UAV's inertia now plays a role in the dynamics of the interaction. These characteristics are now taken into account when selecting the interaction strategy to achieve high frequencies or large oscillation amplitudes. Summarizing, the main novelties of this paper with respect to our previous work [10] are the following:

- Generalization of the shaking controller to consider interactions through translation or rotational movements.
- Theoretical analysis and experimental validation of the two interaction strategies.

This new approach brings us closer to the practical use of aerial manipulators for fruit collection through tree shaking, as it allows us to analyze the interaction with the tree based on the platform's characteristics. The analysis now focuses on a specific point, possibly the only accessible one on the tree.

The remainder of the paper is organized as follows. Sec. II presents the models of the aerial manipulator and the tree, while Sec. III outlines the complete control framework used for shaking trees. Then, by integrating the tree and UAV models with the control framework, Sec. IV analyzes in detail the closed-loop dynamics achieved during the UAV-tree interaction, and it presents the advantages and disadvantages of the two shaking strategies. This analysis is compared with the experimental results in Sec. V. Finally, the conclusions of this work are summarized in Sec. VI.

## II. SYSTEM MODELING

### A. Aerial Platform Model

To model the aerial platform, we define a world frame, represented as $\mathcal{F}_{\mathrm{W}}$, with its origin at $O_{\mathrm{W}}$ and axes $\mathbf{x}_{\mathrm{W}}$, $\mathbf{y}_{\mathrm{W}}$, and $\mathbf{z}_{\mathrm{W}}$. We also define a body frame $\mathcal{F}_{\mathrm{B}}$ located at the center of mass $O_{\mathrm{B}}$ of the aerial platform, with axes $\mathbf{x}_{\mathrm{B}}$, $\mathbf{y}_{\mathrm{B}}$, and $\mathbf{z}_{\mathrm{B}}$.

The position and orientation of the platform with respect to $\mathcal{F}_{\mathrm{W}}$ are given by $\mathbf{p}_{\mathrm{B}} = [x, y, z]^{\top} \in \mathbb{R}^3$ and ${}^{\mathrm{W}}\mathbf{R}_{\mathrm{B}} \in \mathsf{SO}(3)$, respectively. Based on these, we define the linear velocity $\dot{\mathbf{p}}_{\mathrm{B}} \in \mathbb{R}^3$ and angular velocity $\boldsymbol{\omega}_{\mathrm{B}} \in \mathbb{R}^3$ expressed in $\mathcal{F}_{\mathrm{B}}$, which are combined to form the system's twist, $\mathbf{v}_{\mathrm{B}} \in \mathbb{R}^6$. Additionally, we assume the platform has fully-actuated capabilities, so it can generate a complete control wrench $\boldsymbol{\tau}_{\mathrm{c}} \in \mathbb{R}^6$. With this, the Lagrangian model of the aerial platform is:

$$\mathbf{M}_{\mathrm{B}}\dot{\mathbf{v}}_{\mathrm{B}} + \mathbf{c}\left(\boldsymbol{\omega}_{\mathrm{B}}\right) + \mathbf{g}\left({}^{\mathrm{W}}\mathbf{R}_{\mathrm{B}}\right) = \boldsymbol{\tau}_{\mathrm{c}} + \boldsymbol{\tau}_{\mathrm{ext}}, \tag{1}$$

where $\mathbf{M}_{\mathrm{B}} \in \mathbb{R}^{6\times6}$ represents the constant inertia matrix in the body frame, $\mathbf{c}\left(\boldsymbol{\omega}_{\mathrm{B}}\right) \in \mathbb{R}^6$ is the Coriolis force vector, $\mathbf{g}\left({}^{\mathrm{W}}\mathbf{R}_{\mathrm{B}}\right) \in \mathbb{R}^6$ denotes the gravitational wrench, and $\boldsymbol{\tau}_{\mathrm{ext}} \in \mathbb{R}^6$ is the external wrench exerted on the system due to interactions with the environment. Fig. 2-a shows the aerial platform with the needed frames while interacting with a tree.

### B. Tree Model

To model the tree, we use a reference frame denoted as $\mathcal{F}_{\mathrm{T}}$, with its origin $O_{\mathrm{T}}$ located at the base of the tree. The axes of this frame are $\mathbf{x}_{\mathrm{T}}$, $\mathbf{y}_{\mathrm{T}}$, and $\mathbf{z}_{\mathrm{T}}$, where $\mathbf{z}_{\mathrm{T}}$ points in

the direction opposite to gravity, while $\mathbf{x}_\mathrm{T}$ is aligned with the direction of the tree movement, generated by the UAV interaction, and defines an angle $\delta$ with $\mathbf{x}_\mathrm{W}$. Note that the frame orientation depends on the shaking direction.

To model the dynamic behavior of trees, three primary approaches are commonly employed [11]: $(i)$ the lumped-mass method, $(ii)$ the beam with distributed mass model, and $(iii)$ the finite element method (FEM). Among these, FEM offers the highest accuracy and modeling flexibility; however, it necessitates computational analysis due to the complexity of the calculations involved. The beam with distributed mass approach represents the trunk as a continuous beam with distributed mass. While the system's response can be derived by solving the associated partial differential equations, analytical solutions are only attainable in simplified cases. Lastly, the lumped-mass method reduces the system to a discrete model, typically represented as a 1DoF mass-spring-damper system, providing a simplified yet insightful approximation.

In our case, the dynamic model is derived using the Rayleigh-Ritz method, which allows the continuous system to be modeled as a 1-DoF system, similarly to the lumped-mass method. Although FEM would allow for the inclusion of complex effects such as fruit–branch dynamics or wind interaction, this 1-DoF representation is particularly convenient for analytical analysis, offering an efficient alternative compared to more complex methods such as FEM or the distributed mass beam model. Moreover, unlike the lumped-mass approach, the Rayleigh-Ritz method enables the interaction point to be incorporated into the formulation by adjusting the equivalent parameters of the resulting model.

In the following, we present the 1DoF model of the tree (Sec. II-B.1). Based on this, we derive the tree's kinematics (Sec. II-B.2), which are needed to compute the displacement, velocity, and acceleration at any point on the tree.

*1) 1DoF Mass-Spring-Damper Model:* The tree is composed of three main elements: the trunk, the $n_\mathrm{B} \in \mathbb{N}$ branches connected to the trunk, and the $n_\mathrm{F} \in \mathbb{N}$ fruits. The trunk is modeled as a flexible element, while the branches are treated as rigid elements, and the fruits are considered as point masses. For simplicity, we assume that the trunk is in a vertical position with a total length $l_T \in \mathbb{R}^+$, while the branches are modeled as straight elements connected to the trunk. Note that this simplification does not limit our approach, as more complex geometries can be considered by introducing their parametrized curves in the computation of the equivalent mass, as shown in our previous work [10]. To avoid over-extension of the current model, readers can refer to our previous work for a more detailed treatment of these more complex shapes. The main parameters of the trunk are its linear density $\rho_T \in \mathbb{R}^+$, Young's modulus $E \in \mathbb{R}^+$, and its cross-sectional moment of inertia $I \in \mathbb{R}^+$, needed in the dynamic model. Each branch $B_i$ has a linear density $\rho_{B_i} \in \mathbb{R}^+$ with a total length of $l_{B_i} \in \mathbb{R}^+$, and is embedded in the trunk at height $z_{B_i} \in \mathbb{R}^+$ from the ground. Each branch forms an angle $\beta_{B_i} \in \mathbb{R}$ with the ground plane $\mathbf{x}_\mathrm{T}\mathbf{y}_\mathrm{T}$, while its projection onto the movement plane $\mathbf{x}_\mathrm{T}\mathbf{y}_\mathrm{T}$ defines

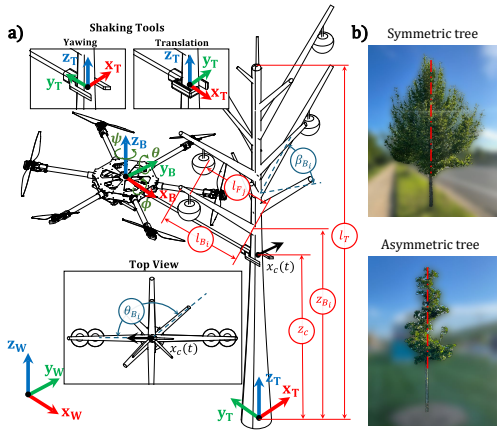


Fig. 2. a) Aerial manipulator physically interacting with a tree, including frames and magnitudes. Two shaking tools can be used: one for yawing interactions and another for translational interactions. b) Symmetric tree (top) and asymmetric tree (bottom). Note that even if the tree is asymmetric, it does not severely affect the symmetry, as Eq. (2) can still represent a tree branch.

an angle $\theta_{B_i} \in \mathbb{R}$ relative to $\mathbf{x}_\mathrm{T}$. Each fruit $F_j$ has a mass $m_{F_j} \in \mathbb{R}^+$ and is located on the branch $B_i$ at a distance $l_{F_j} \in \mathbb{R}^+$ along the branch. This modeling framework of trunk, branches and fruits enables the computation of the equivalent mass, stiffness, and damping parameters of the system required in the 1DoF model. Fig. 2-a illustrates the tree with all these geometric characteristics.

The selected degree of freedom is the displacement $x_c(t) \in \mathbb{R}$ of the contact point through which the UAV interacts with the tree. This point is positioned at a height $z_c \in \mathbb{R}^+$ along the trunk, as shown in Fig. 2-a. Although the model assumes interaction through the trunk, it can also be applied at the branch level if the trunk is sufficiently rigid and can be considered a fixed base. This allows the use of our work even when aerial manipulators lack the force to shake the trunk directly, by instead targeting individual branches. With all this, the dynamic model remains:

$$m^{\mathrm{eq}}\ddot{x}_c(t) + c^{\mathrm{eq}}\dot{x}_c(t) + k^{\mathrm{eq}}x_c(t) = f^x_{\mathrm{tree}}(t), \qquad (2)$$

where $f^x_{\mathrm{tree}}(t) \in \mathbb{R}$ is the force applied by the UAV onto the tree trunk in the $\mathbf{x}_\mathrm{T}$ direction, and $m^{\mathrm{eq}} \in \mathbb{R}^+$, $c^{\mathrm{eq}} \in \mathbb{R}^+$ and $k^{\mathrm{eq}} \in \mathbb{R}^+$ represent the equivalent mass, equivalent damping, and equivalent stiffness of the tree, respectively. These equivalent parameters depend on the characteristics of the trunk, branches, and fruits. The calculations for determining these parameters are thoroughly detailed in our prior work [10].

*2) Tree Kinematics:* The Rayleigh-Ritz method allows for calculating the position $\mathbf{p}_T(\lambda) \in \mathbb{R}^3$ of any point along the trunk using a shape function $\eta(\lambda) \in \mathbb{R}$, where $\lambda \in [0, l_T]$ parametrizes the position along the length of the tree. This shape function represents the shape of the first vibration mode of the flexible trunk, and it is presented in [10]. Using this, $\mathbf{p}_T(\lambda)$ remains:

$$\mathbf{p}_T(\lambda) = x_c\eta(\lambda)\mathbf{x}_\mathrm{T} + \lambda\mathbf{z}_\mathrm{T}, \qquad (3)$$

which shows that the motion occurs in the $\mathbf{x}_\mathrm{T}\mathbf{z}_\mathrm{T}$ plane. Considering this, the position $\mathbf{p}_{B_i}(z_{B_i}, \mu)$ of any point $\mu \in [0, l_{B_i}]$ of a branch $B_i$ is computed as:

$$\mathbf{p}_{B_i}(z_{B_i}, \mu) = \mathbf{p}_T(z_{B_i}) + \mu \mathbf{u}_{B_i} + x_c \eta'_{z_{B_i}} \mathbf{y}_\mathrm{T} \times \mu \mathbf{u}_{B_i}, \quad (4)$$

where $\eta'_{z_{B_i}} = \frac{\partial \eta(\lambda)}{\partial \lambda}|_{\lambda = z_{B_i}}$ accounts for the rotation of the trunk section at the junction with branch $B_i$ due to trunk deformation, and $\mathbf{u}_{B_i} \in \mathbb{R}^3$ is the unit direction vector along branch $B_i$. The displacement of any point on the branch $B_i$ is expressed as $\Delta\mathbf{p}_{B_i} = \mathbf{p}_{B_i} - \mathbf{p}^0_{B_i}$, where $\mathbf{p}^0_{B_i}$ is obtained by evaluating Eq. (4) without trunk deformation $\eta(\lambda) = 0$, $\forall \lambda \in [0, l_T]$. This results in the following expression:

$$\Delta\mathbf{p}_{B_i}(z_{B_i}, \mu) = x_c \underbrace{\left(\eta(z_{B_i})\mathbf{x}_\mathrm{T} + \eta'_{z_{B_i}} \mathbf{y}_\mathrm{T} \times \mu \mathbf{u}_{B_i}\right)}_{\mathbf{t}_\mathrm{Tree}}, \quad (5)$$

where the term $\mathbf{t}_\mathrm{Tree}$ depends only on the tree geometry. Moreover, by derivation of Eq. (4) we obtain the velocity and acceleration of any point of the tree as:

$$\dot{\mathbf{p}}_{B_i}(z_{B_i}, \mu) = \dot{x}_c \mathbf{t}_\mathrm{Tree} \quad \text{and} \quad \ddot{\mathbf{p}}_{B_i}(z_{B_i}, \mu) = \ddot{x}_c \mathbf{t}_\mathrm{Tree}. \quad (6)$$

These expressions show that the displacement, velocity, and acceleration of any point on the tree are proportional to those at the contact point. Finally, the position $\mathbf{p}_{F_j}$, velocity $\dot{\mathbf{p}}_{F_j}$ and acceleration $\ddot{\mathbf{p}}_{F_j}$ of the fruit $F_j$ in branch $B_i$ are computed using Eq. (4) and Eq. (6) with $\mu = l_{F_j}$.

## III. CONTROL

The aerial manipulator control framework for shaking trees is based on a hybrid pose/shaking controller. Fig. 3 gives an overview of the control framework.

The hybrid pose/shaking controller allows shaking in specific directions while maintaining stable positioning in the other directions [12]. The hybrid pose/shaking controller is:

$$\boldsymbol{\tau}_\mathrm{c} = \boldsymbol{\Lambda}\boldsymbol{\tau}_f + (\mathbf{I} - \boldsymbol{\Lambda})\,\boldsymbol{\tau}_p + \mathbf{c}\,(\boldsymbol{\omega}_\mathrm{B}) + \mathbf{g}\left({}^\mathrm{W}\mathbf{R}_\mathrm{B}\right), \quad (7)$$

where $\boldsymbol{\Lambda} = \mathrm{diag}\,(\boldsymbol{\lambda}) \in \mathbb{R}^{6\times6}$ is a diagonal, binary selection matrix where each element of the selection vector $\boldsymbol{\lambda} \in \mathbb{R}^6$ is either one or zero, indicating whether shaking control $\boldsymbol{\tau}_f$ or position control $\boldsymbol{\tau}_p$ is enabled for each respective axis. This matrix allows for selecting the shake direction of the UAV. The remaining terms compensate Coriolis and gravity wrenches.

### A. Pose Controller

The pose controller implements a PD control strategy as:

$$\boldsymbol{\tau}_p = \mathbf{K}_P\tilde{\mathbf{e}} + \mathbf{K}_D\dot{\tilde{\mathbf{e}}}, \quad (8)$$

with $\mathbf{K}_D, \mathbf{K}_P \in \mathbb{R}^{6\times6}$ being positive definite gain matrices, $\tilde{\mathbf{e}} = \left[\mathbf{e}_p^\top\ \mathbf{e}_R^\top\right]^\top \in \mathbb{R}^6$ the stacked pose error vector, and $\dot{\tilde{\mathbf{e}}}$ its derivative. The position error $\mathbf{e}_p$ and orientation error $\mathbf{e}_R$ are computed as the following geometric errors:

$$\mathbf{e}_p = {}^\mathrm{W}\mathbf{R}_\mathrm{B}^\top\left(\mathbf{p}_\mathrm{W}^\mathrm{ref} - \mathbf{p}_\mathrm{W}\right), \quad (9a)$$

$$\mathbf{e}_R = \frac{1}{2}\,\mathrm{vec}\left({}^\mathrm{W}\mathbf{R}_\mathrm{B}^\top {}^\mathrm{W}\mathbf{R}_\mathrm{B}^\mathrm{ref} - {}^\mathrm{W}\mathbf{R}_\mathrm{B}^{\mathrm{ref}\top} {}^\mathrm{W}\mathbf{R}_\mathrm{B}\right), \quad (9b)$$

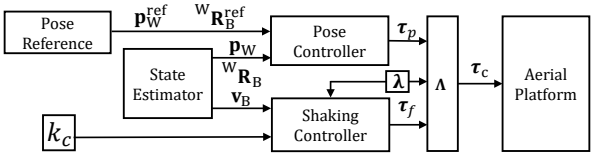


Fig. 3. Control scheme with the main components.

with $\mathbf{p}_\mathrm{W}^\mathrm{ref}$ and ${}^\mathrm{W}\mathbf{R}_\mathrm{B}^\mathrm{ref}$ representing the reference position and orientation, $\mathbf{p}_\mathrm{W}$ the UAV position in $\mathcal{F}_\mathrm{W}$, and $\mathrm{vec}\,(*)$ the operator used to extract a vector from a skew-symmetric matrix.

### B. Shaking Controller

To shake the tree, we employ a self-excited oscillation strategy [13]. This feedback control force generates self-excited oscillations at the system's natural frequency [14]. The shaking controller works by applying a control wrench, $\boldsymbol{\tau}_f$, which always has the same sign as the velocity in the shaking direction. In this way, the UAV continuously injects energy into the tree, resulting in oscillatory movement. The control law is:

$$\boldsymbol{\tau}_f = k_c\,\mathrm{sgn}\left(\boldsymbol{\lambda}^\top\mathbf{v}_\mathrm{B}\right)\boldsymbol{\lambda}, \quad (10)$$

where sgn is the signum function and the shaking control gain $k_c \in \mathbb{R}^+$ allows control over the amplitude of the oscillatory motion. In this case, we assume that the UAV shakes in only one direction, so the selection vector $\boldsymbol{\lambda}$ has only one nonzero element. This decoupled formulation was intentionally chosen to enable independent validation and analysis of each shaking strategy. A hybrid strategy combining both modes is proposed as future work. Both variables, the shaking control gain $k_c$ and the selection vector $\boldsymbol{\lambda}$, are chosen by the user to interact with specific forces/torques and through a specific strategy. Moreover, as Eq. (10) shows, the control law does not require any prior knowledge of the dynamics of the system being shaken; it only depends on the platform velocity $\mathbf{v}_\mathrm{B}$, which can be easily estimated or measured using onboard sensors.

Note that the shaking controller in Eq. (10) can be applied to any flexible system that needs to be driven into resonance, and not only to trees. For example, it could be used to excite a suspended payload or a swing into resonance [15], to stimulate flexible structures such as beams or poles for testing purposes [16]. Despite its broader applicability, this work focuses exclusively on tree shaking.

## IV. ANALYSIS OF CLOSED-LOOP DYNAMICS

This section analyzes the interaction between the aerial manipulator and the tree using the hybrid pose-shaking controller. First, we derive the closed-loop dynamics of the complete system with two strategies: shaking interactions through translations along $\mathbf{x}_\mathrm{B}$, and shaking interactions through yaw rotations about $\mathbf{z}_\mathrm{B}$. Then, we analyze the oscillations achieved in each scenario, including their frequency, displacement, velocities, and accelerations. Although this paper focuses on the controlled shaking of trees, the

following analysis can also be applied to the controlled shaking of other flexible elements, as long as their model is represented by a mass-spring-damper system, similar to Eq. (2).

### A. Closed-Loop Dynamics

For deriving the closed-loop dynamics of the system we introduce the hybrid pose-shaking controller Eq. (7) in the UAV model Eq. (1). Doing this, the UAV closed-loop dynamics is:

$$\mathbf{M}_{\mathrm{B}}\dot{\mathbf{v}}_{\mathrm{B}} = \underbrace{\boldsymbol{\Lambda}\boldsymbol{\tau}_f + (\mathbf{I}-\boldsymbol{\Lambda})\,\boldsymbol{\tau}_p}_{\boldsymbol{\tau}_{\mathrm{pr}}} + \boldsymbol{\tau}_{\mathrm{ext}}, \tag{11}$$

where $\boldsymbol{\tau}_{\mathrm{pr}} = [f^x_{\mathrm{pr}}, f^y_{\mathrm{pr}}, f^z_{\mathrm{pr}}, \tau^x_{\mathrm{pr}}, \tau^y_{\mathrm{pr}}, \tau^z_{\mathrm{pr}}]^\top \in \mathbb{R}^6$ is the control wrench applied by the propellers for controlling the pose or the shaking force. We consider that the pose controller performs well in the specified directions, allowing the UAV to reach the desired pose. In the following, we analyze the two possible scenarios for the UAV's interaction directions with the tree.

**Assumption 1.** *In the following analysis, although our model [10] indicates that the equivalent parameters $m^{\mathrm{eq}}$, $c^{\mathrm{eq}}$, and $k^{\mathrm{eq}}$ depend on the direction of shaking due to the radial distribution of branches and fruits around the trunk, we assume that these parameters are independent of the direction of vibration. In practice, since the branches and fruits of a tree are almost uniformly distributed around the trunk (see Fig. 2-b), the equivalent parameters will be effectively independent of the shaking direction parametrized by $\delta$.*

Note that Assump. 1 does not limit the applicability of our analysis but rather simplifies it. The analysis can be extended to asymmetric trees by explicitly incorporating the shaking direction $\delta$ as a variable. However, such an extension would result in expressions that are highly dependent on the specific tree geometry, making it difficult to perform a general analytical treatment. For this reason, we adopt Assump. 1 to enable a more generic and tractable analysis.

*1) Translation interactions along $\mathbf{x}_{\mathrm{B}}$:* In this case the UAV pull and push the tree in $\mathbf{x}_{\mathrm{B}}$, which is aligned with $\mathbf{x}_{\mathrm{T}}$ . The closed-loop dynamics for the UAV in this direction remains:

$$m_{\mathrm{AM}}\ddot{x} = f^x_{\mathrm{pr}} + f^x_{\mathrm{ext}}, \tag{12}$$

where $m_{\mathrm{AM}} \in \mathbb{R}^+$ is the aerial manipulator mass, and $f^x_{\mathrm{pr}}$ and $f^x_{\mathrm{ext}}$ are the forces applied by the propellers and the external force suffered by the UAV in the $\mathbf{x}_{\mathrm{B}}$ direction, respectively. As $\mathbf{x}_{\mathrm{T}}$ and $\mathbf{x}_{\mathrm{B}}$ are aligned, the movements of the tree and the UAV along $\mathbf{x}_{\mathrm{T}}$ are the same $x(t) = x_c(t)$. Furthermore, according to the principle of action and reaction, the force exerted on the tree is $f^x_{\mathrm{tree}}(t) = -f^x_{\mathrm{ext}}(t)$. With this, the closed-loop dynamics is derived by introducing Eq. (12) in Eq. (2), resulting in the following 1DoF equation:

$$(m^{\mathrm{eq}} + m_{\mathrm{AM}})\ddot{x}_c(t) + c^{\mathrm{eq}}\dot{x}_c(t) + k^{\mathrm{eq}}x_c(t) = f^x_{\mathrm{pr}}(t). \tag{13}$$

Then, the wrench applied by the propellers $\boldsymbol{\tau}_{\mathrm{pr}}$ is a square trajectory defined by the shaking controller (see Eq. (10)). As $\boldsymbol{\lambda} = [1,0,0,0,0,0]^\top$, the force generated by the propellers is $f^x_{\mathrm{pr}} = k^x_c\,\mathrm{sgn}(\dot{x}_c)$. Introducing this in Eq. (13), and solving the differential equation using the averaging method [17], the closed-loop results in $x_c(t) = X_x\cos(\omega_x t)$, with:

$$X_x = \frac{4k^x_c}{\pi c^{\mathrm{eq}}\omega_x} \;\text{ and }\; \omega_x = \sqrt{\frac{k^{\mathrm{eq}}}{m^{\mathrm{eq}} + m_{\mathrm{AM}}}}. \tag{14}$$

Here, $k^x_c$ is the shaking control gain when interacting with the tree through $\mathbf{x}_{\mathrm{B}}$ translations.

*2) Rotation interactions along $\mathbf{z}_{\mathrm{B}}$:* In this case the UAV interacts with the tree through yaw rotations, resulting in a tree movement that aligns $\mathbf{x}_{\mathrm{T}}$ with $\mathbf{y}_{\mathrm{B}}$. The closed-loop dynamics of the UAV in this direction remains:

$$I_{\mathrm{zz}}\ddot{\psi} = \tau^z_{\mathrm{pr}} + \tau^\psi_{\mathrm{ext}}, \tag{15}$$

where $\psi \in \mathbb{R}$ is the yaw angle, $I_{\mathrm{zz}} \in \mathbb{R}^+$ is the aerial manipulator inertia around $\mathbf{z}_{\mathrm{B}}$, and $\tau^z_{\mathrm{pr}}$ and $\tau^\psi_{\mathrm{ext}}$ are the torques applied by the propellers and the external torque suffered by the UAV around the $\mathbf{z}_{\mathrm{B}}$ direction, respectively. As $\mathbf{x}_{\mathrm{T}}$ and $\mathbf{y}_{\mathrm{B}}$ are aligned, the movement of the tree coincides with the motion in $\mathbf{y}_{\mathrm{B}}$ at the interaction point of the UAV tool $y_{\mathrm{tool}}(t) = x_c(t)$. Furthermore, the movement at the tool tip is related to the yaw through $y_{\mathrm{tool}}(t) = x_c(t) = \psi(t)L$, where $L \in \mathbb{R}^+$ represents the distance from the center of mass (CoM) to the interaction point. With this, and introducing Eq. (15) in Eq. (2), the closed-loop dynamics remains:

$$\left(m^{\mathrm{eq}} + \frac{I_{\mathrm{zz}}}{L^2}\right)\ddot{x}_c(t) + c^{\mathrm{eq}}\dot{x}_c(t) + k^{\mathrm{eq}}x_c(t) = \frac{\tau^z_{\mathrm{pr}}(t)}{L}, \tag{16}$$

where we have applied the action-reaction principle with $f^x_{\mathrm{tree}}(t)L = -\tau^\psi_{\mathrm{ext}}(t)$. Similarly to the previous case, the torque from the propellers follows the reference of the shaking controller $\tau^z_{\mathrm{pr}} = k^\psi_c\,\mathrm{sgn}(\dot{\psi})$, as $\boldsymbol{\lambda} = [0,0,0,0,0,1]^\top$. Doing this, and as $\mathrm{sgn}(\dot{\psi}) = \mathrm{sgn}(\dot{x}_c)$, the closed-loop results in an oscillatory motion $x_c(t) = X_\psi\cos(\omega_\psi t)$, with:

$$X_\psi = \frac{4k^\psi_c}{\pi L c^{\mathrm{eq}}\omega_\psi} \;\text{ and }\; \omega_\psi = \sqrt{\frac{k^{\mathrm{eq}}}{m^{\mathrm{eq}} + I_{\mathrm{zz}}/L^2}}. \tag{17}$$

Here, $k^\psi_c$ is the shaking control gain when interacting with the tree through yaw rotations around $\mathbf{z}_{\mathrm{B}}$.

### B. Frequency

The oscillation frequencies are independent of the shaking control gains, as shown in Eq. (14) and Eq. (17). To achieve higher frequencies by $\mathbf{x}_{\mathrm{B}}$ translation than by $\psi$ rotation $\omega_x \geq \omega_\psi$, the following condition must be satisfied:

$$\omega_x \geq \omega_\psi \Leftrightarrow \sqrt{\frac{k^{\mathrm{eq}}}{m^{\mathrm{eq}} + m_{\mathrm{AM}}}} \geq \sqrt{\frac{k^{\mathrm{eq}}}{m^{\mathrm{eq}} + I_{\mathrm{zz}}/L^2}}. \tag{18}$$

This condition is satisfied when $m_{\mathrm{AM}} \leq I_{\mathrm{zz}}/L^2$, which depends only on the UAV itself, and not on the shaken system. Therefore, depending on the aerial manipulator used, it may be preferable to excite by translation or by rotation to achieve higher oscillation frequencies. For instance, when

the tree has a dense canopy that prevent entry into the tree, a long arm of length $L$ is required to interact with the trunk. Furthermore, aerial platforms with mass highly concentrated in the center result in low-inertia $I_{zz}$ designs. In such cases, $m_{\mathrm{AM}} \leq I_{zz}/L^2$ may not be satisfied, resulting in $\omega_x \leq \omega_\psi$.

### C. Oscillation Amplitude

The oscillation amplitudes depend linearly on the shaking gain, as shown in Eq. (14) and Eq. (17). To analyze the possible shaking strategies independently of the control gain, we first examine the case where the system is excited with the same force $f^x_{\mathrm{tree}}$. Comparing Eq. (13) and Eq. (16), this occurs when $k^x_c L = k^\psi_c$. Considering this, to achieve higher oscillation amplitudes by $\mathbf{x}_\mathrm{B}$ translation than by $\psi$ rotation $X_x \geq X_\psi$, the following condition must be satisfied:

$$X_x \geq X_\psi \Leftrightarrow \frac{4k^x_c}{\pi c^{\mathrm{eq}} \omega_x} \geq \frac{4k^\psi_c}{\pi L c^{\mathrm{eq}} \omega_\psi} \Leftrightarrow \omega_\psi \geq \omega_x, \tag{19}$$

where we have considered $k^x_c L = k^\psi_c$. As shown in Sec. IV-B, this condition is satisfied when $m_{\mathrm{AM}} \geq I_{zz}/L^2$. Therefore, similarly to the oscillation frequency, this condition depends only on the chosen UAV and not on the shaken system.

### D. Velocity

As the resulting movement is an oscillatory movement, the velocities are obtained as $\dot{x}_c(t) = -\omega x_c(t)$. To obtain higher velocity amplitudes for $\mathbf{x}_\mathrm{B}$ translation compared to $\psi$ rotation $\dot{X}_x \geq \dot{X}_\psi$, the following condition must be satisfied:

$$\dot{X}_x \geq \dot{X}_\psi \Leftrightarrow \frac{4k^x_c \omega_x}{\pi c^{\mathrm{eq}} \omega_x} \geq \frac{4k^\psi_c \omega_\psi}{\pi L c^{\mathrm{eq}} \omega_\psi} \Leftrightarrow 1 \geq 1, \tag{20}$$

where we have considered $k^x_c L = k^\psi_c$. In this case, there is no difference between shaking the system through translation or through rotation, as the velocity amplitudes will be the same.

### E. Acceleration

The accelerations in oscillatory motion are expressed as $\ddot{x}_c(t) = -\omega^2 x_c(t)$. To achieve higher acceleration amplitudes for $\mathbf{x}_\mathrm{B}$ translation compared to $\psi$ rotation, the following condition must be satisfied:

$$\ddot{X}_x \geq \ddot{X}_\psi \Leftrightarrow \frac{4k^x_c \omega_x^2}{\pi c^{\mathrm{eq}} \omega_x} \geq \frac{4k^\psi_c \omega_\psi^2}{\pi L c^{\mathrm{eq}} \omega_\psi} \Leftrightarrow \omega_x \geq \omega_\psi, \tag{21}$$

where we have considered $k^x_c L = k^\psi_c$. This condition is satisfied when $m_{\mathrm{AM}} \leq I_{zz}/L^2$, and depends only on the UAV.

### F. Summary Comparison

Table I summarizes the conditions for achieving higher frequency, displacement, velocity, and acceleration depending on the shaking strategy. Furthermore, the relation between each magnitude of each method can be expressed as:

$$\frac{\omega_x}{\omega_\psi} = \beta, \ \frac{X_x}{X_\psi} = \frac{1}{\beta}, \ \frac{\dot{X}_x}{\dot{X}_\psi} = 1, \ \text{and} \ \frac{\ddot{X}_x}{\ddot{X}_\psi} = \beta, \tag{22}$$

where $\beta = \sqrt{\dfrac{m^{\mathrm{eq}} + I_{zz}/L^2}{m^{\mathrm{eq}} + m_{\mathrm{AM}}}}$. These results indicate an inverse relationship between high oscillation frequencies and large displacements. For a given UAV a strategy that achieves high frequencies results in lower displacements, and vice versa. This helps in selecting the appropriate strategy based on the task. For example, if the objective is a health monitoring task, such as assessing trunk flexibility [18], higher amplitudes are needed, whereas for fruit harvesting [5], higher frequencies are preferred. Note that the selection depends only on the platform parameters ($m_{\mathrm{AM}}, L$, and $I_{zz}$) and does not require any information about the tree. However, if one wants to estimate the exact closed-loop amplitude and oscillation frequency before interacting with the tree, knowledge of the tree parameters is necessary. These parameters can be obtained using tree morphology identification techniques [19], fruit position estimation methods [20], or mechanical property databases [21].

TABLE I

SUMMARY COMPARISON WITH $k^x_c L = k^\psi_c$.

| **Magnitude** | $\mathbf{x}_\mathrm{B}$ Tran. | $\mathbf{z}_\mathrm{B}$ Rot. |
|---|---|---|
| **Frequency** | $\omega_x \geq \omega_\psi$ if $m_{\mathrm{AM}} \leq I_{zz}/L^2$ | |
| **Displacement** | $X_x \geq X_\psi$ if $m_{\mathrm{AM}} \geq I_{zz}/L^2$ | |
| **Velocity** | $\dot{X}_x = \dot{X}_\psi$ always | |
| **Acceleration** | $\ddot{X}_x \geq \ddot{X}_\psi$ if $m_{\mathrm{AM}} \leq I_{zz}/L^2$ | |

## V. EXPERIMENTAL VALIDATION

### A. Description

For experimental validation, we used an Omnidirectional Micro Aerial Vehicle (OMAV) [12]. This platform has

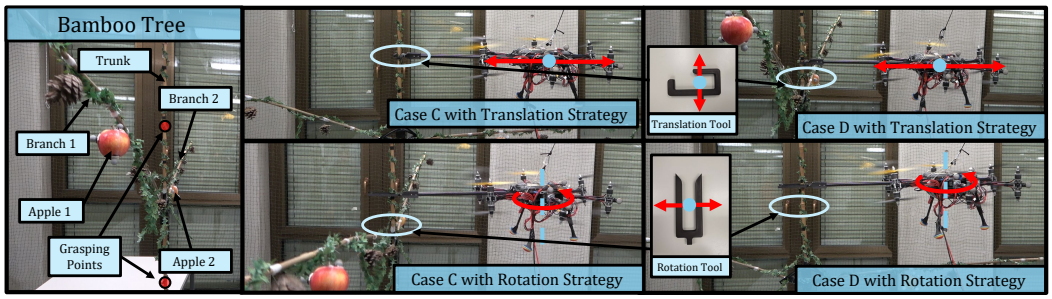


Fig. 4. Experimental setup with the bamboo tree consisting of a trunk and two branches. Case C, where $z_c = 1$ m and $\delta = 0°$, for the two shaking strategies. Case D, where $z_c = 1$ m and $\delta = 90°$, for the two shaking strategies. The shaking tools are also included for each strategy.

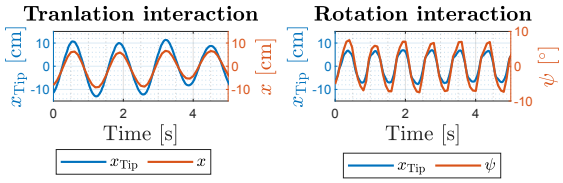


Fig. 5. Results of the interaction strategies. Top: results of the translational interactions, with the achieved oscillations at the tree tip $x_{\mathrm{Tip}}$ (blue) and the displacement of the robot $x$ for shaking the tree (orange). Bottom: results of the rotational interactions, with the achieved oscillations at the tree tip $x_{\mathrm{Tip}}$ (blue) and the yaw movement of the robot $\psi$ for shaking the tree (orange).

$m_{\mathrm{AM}} = 2.5$ kg and $I_{\mathrm{zz}} = 0.15\ \mathrm{kg\,m^2}$, with the interaction tool installed at $L = 0.50$ m. We use two tools for interaction through $\mathbf{x}_{\mathrm{B}}$ displacement and $\psi$ rotations, as shown in Fig. 2-a.

The tree used is a handmade bamboo tree composed of a trunk, two branches, and two fruits, as shown in Fig. 4. This setup enables precise control over the system parameters, allowing us to evaluate the $\beta$ estimations and compare them with the experimental results $\beta_{\mathrm{exp}}$ without introducing significant parameter uncertainties. If a real tree is used for validation, the required parameters can be obtained through state-of-the-art methods, as indicated at the end of Sec. IV-F.

Due to the lack of numerous branches and fruits distributed uniformly around the trunk, this tree does not satisfy Assump. 1. In this case, $m^{\mathrm{eq}}, c^{\mathrm{eq}}, k^{\mathrm{eq}}$ depend not only on the interaction point but also on the shaking direction $\delta$. However, we exploit this possibility to have more validation cases with different parameters, testing two shaking directions $\delta$ for each interaction point. We perform experiments by interacting with the tree at two distinct points $z_c$ and with two different shaking directions $\delta$, resulting in four unique cases. For each case, both strategies are compared under the same shaking directions.

We compute the equivalent mass $m^{\mathrm{eq}}$ needed for the $\beta$ estimations using $z_c$ and $\delta$ of each case[1]. For each case listed in Tab. II, we evaluate both interaction strategies using different control gains $k_c$. As done in Sec. IV, we interact with the tree with the same force, as $k_c = k_c^x = k_c^\psi / L$. Fig. 4 shows cases C and D for the translation and rotation strategies.

TABLE II

POSITION AND SHAKING DIRECTION OF THE EXPERIMENTAL CASES.

| Case | A | B | C | D |
|---|---|---|---|---|
| $z_c$ | 0.25 m | 0.25 m | 1.00 m | 1.00 m |
| $\delta$ | 0.0° | 90.0° | 0.0° | 90.0° |

### B. Shaking Controller Validation

First, we validate the proposed control framework interacting with the tree through both strategies. Fig. 5 shows the results when the UAV interacts with the tree under the conditions of Case C, with a control gain of $k_c = 0.6$ N. In particular, Fig. 5 (left) shows the position of the UAV and the tree tip for the translational strategy, which generates vibrations through $\mathbf{x}_{\mathrm{B}}$ movement. Similarly, Fig. 5 (right) shows the yaw angle of the UAV and the position of the tree tip for the rotational strategy, where rotational movements also induce vibrations in the tree but now due to $\psi$ rotations.

[1]For further details on the computation of $m^{\mathrm{eq}}$, refer to [10].

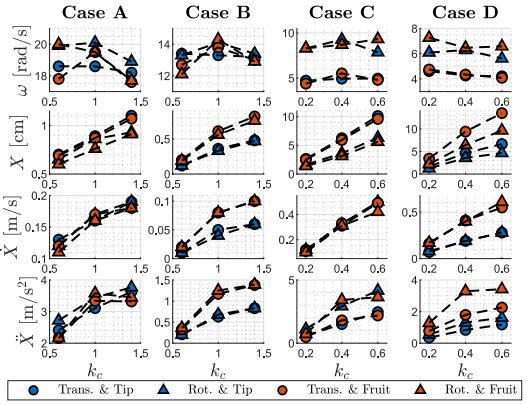


Fig. 6. Experimental results for the four cases. Circles represent the results using the translation strategy, while triangles indicate the rotation strategy. Blue markers correspond to the measured magnitudes at the tree tip, and red markers to those at the fruit.

### C. Oscillatory Movement

After validating the control framework, we evaluate the oscillatory movement achieved during the interaction, in terms of frequency, amplitude displacement, velocity and acceleration, as presented in Sec. IV. These magnitudes, measured using a motion capture system, are compared for the tree tip and for the fruit 1. The platform interacts with the tree with three different control gains $k_c$ in each case, and with both strategies. The experimental results are summarized in Fig. 6.

As in the OMAV platform we have $m_{\mathrm{AM}} > I_{\mathrm{zz}}/L^2$ ($\beta < 1$), we expect $\omega_\psi > \omega_x$, $X_x > X_\psi$ and $\ddot{X}_\psi > \ddot{X}_x$, as summarized in Tab. I. Comparing these magnitudes in Fig. 6 for each interaction point and across the different shaking strategies, it can be observed that the theoretical estimations are consistent with the experimental results. Specifically, although Fig. 6 only presents experimental data, the linear dependence of displacement, velocity, and acceleration on the control gain $k_c$, as well as the independence of the oscillation frequency from $k_c$, can be clearly observed. These trends are in agreement with the analytical predictions derived in Eq. (14) and Eq. (17).

To compare the experimental results, we compute the estimated $\beta$ parameter for each case. Using the parameters and the tree model [10], the equivalent mass for each case is $m_A^{\mathrm{eq}} = 14.8$ kg, $m_B^{\mathrm{eq}} = 33.5$ kg, $m_C^{\mathrm{eq}} = 0.42$ kg, and $m_D^{\mathrm{eq}} = 1.45$ kg. With this, the estimated $\beta$ values are $\beta_A = 0.94$, $\beta_B = 0.97$, $\beta_C = 0.59$, and $\beta_D = 0.72$. We compute the resulting ratio by dividing the translation results by the rotation results. These ratios are shown in Fig. 7, where the blue and red markers represent the experimental results based on the measurements at the tip and at the fruit, respectively. Furthermore, the stars indicate the theoretical estimations computed using Eq. (22).

As shown in Fig. 7, for cases A and B, the ratio $\beta \approx 1$,

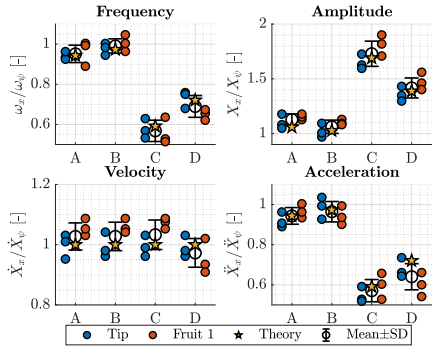


Fig. 7. Theoretical and experimental comparison for the frequency, amplitude, velocity and acceleration at the tip (blue) and fruit (red).

as the equivalent mass $m^{\text{eq}}$ is significantly higher compared to the characteristics of the UAV. In these cases, there is little difference between interacting through translations or rotations, and the results are very similar. However, when the UAV interacts with the tree at the top points (cases C and D), the equivalent mass $m^{\text{eq}}$ decreases, and the UAV's characteristics begin to play a more significant role. Specifically, there are now notable differences in terms of frequency, displacement and accelerations when using one strategy or the other. Furthermore, the experimental results show that our analysis accurately predicts the behavior of the system for both shaking strategies. However, the estimations based on measurements taken at the fruit exhibit greater deviation compared to those taken at the tip. This can be attributed to the fact that the fruit is not rigidly attached to the branch, allowing other modes of vibration to emerge during movement. Additionally, the deviation in the fruit-based estimations is more pronounced in cases C and D, where the displacements are higher, making these other modes more noticeable.

## VI. CONCLUSIONS

This paper presents an analysis of how to use aerial manipulators for shaking trees, along with experimental validation. To achieve this, we have extended our previous shaking control framework to account for interactions through $\mathbf{x}_{\text{B}}$ translations and $\psi$ rotations. The control framework is then integrated with the tree model, yielding the closed-loop dynamics. We analyze these closed-loop dynamics for each control strategy, determining which one is better for achieving high amplitudes or high frequencies. One important conclusion is that, for a given interaction point and force, the decision depends solely on the mass and inertia of the platform. Finally, the theoretical analysis is validated with indoor experiments. The experiments show that when interacting with the lower part of the trunk, the rotation and translation strategies give approximately the same results. However, when interacting with the upper part of the trunk, noticeable differences appear between the two strategies in terms of frequencies, amplitudes, and accelerations.

Future work includes implementing the proposed controlled shaking scheme in outdoor scenarios with real trees, where outdoors factors such as wind may be present. Additionally, future efforts will focus on the development of a hybrid shaking strategy that combines the translational and rotational approaches.

## REFERENCES

[1] A. Ollero, M. Tognon, A. Suarez, *et al.*, "Past, present, and future of aerial robotic manipulators," *IEEE Transactions on Robotics*, vol. 38, no. 1, pp. 626–645, 2021.

[2] A. Ollero, G. Heredia, A. Franchi, *et al.*, "The AEROARMS Project: Aerial Robots with Advanced Manipulation Capabilities for Inspection and Maintenance," *IEEE Robotics Automation Magazine*, vol. 25, no. 4, pp. 12–23, 2018.

[3] H. Yang, N. Staub, A. Franchi, *et al.*, "Modeling and Control of Multiple Aerial-Ground Manipulator System (MAGMaS) with Load Flexibility," in *2018 IEEE/RSJ International Conference on Intelligent Robots and Systems (IROS)*. IEEE, 2018, pp. 1–8.

[4] J. R. Kutia, K. A. Stol, and W. Xu, "Aerial manipulator interactions with trees for canopy sampling," *IEEE/ASME Transactions on Mechatronics*, vol. 23, no. 4, pp. 1740–1749, 2018.

[5] Z. Zhang, C. Igathinathane, J. Li, *et al.*, "Technology progress in mechanical harvest of fresh market apples," *Computers and Electronics in Agriculture*, vol. 175, p. 105606, 2020.

[6] C. Ortiz, A. Torregrosa, and S. C. García, "Comparison of a lightweight experimental shaker and an orchard tractor mounted trunk shaker for fresh market citrus harvesting," *Agriculture*, vol. 11, no. 11, 2021.

[7] I. Kovacic, D. Radomirovic, and M. Zukovic, "Tree vibrations: Determining oscillatory properties by using infra-red marker-tracking system," *Urban Forestry & Urban Greening*, vol. 34, pp. 114–120, 2018.

[8] E. Grande, E. Giordano, and F. Clementi, "Evaluation of dynamic properties of trees subjected to induced vibrations," *Applied Sciences*, vol. 13, no. 12, 2023.

[9] E. Aucone, S. Kirchgeorg, A. Valentini, *et al.*, "Drone-assisted collection of environmental dna from tree branches for biodiversity monitoring," *Science Robotics*, vol. 8, no. 74, p. eadd5762, 2023.

[10] A. González-Morgado, E. Cuniato, M. Tognon, *et al.*, "Controlled shaking of trees with an aerial manipulator," *IEEE/ASME Transactions on Mechatronics*, pp. 1–12, 2024.

[11] K. R. James, G. A. Dahle, J. Grabosky, *et al.*, "Tree biomechanics literature review: Dynamics," *Arboriculture & Urban Forestry (AUF)*, vol. 40, no. 1, pp. 1–15, 2014.

[12] K. Bodie, M. Brunner, M. Pantic, *et al.*, "An omnidirectional aerial manipulation platform for contact-based inspection." Robotics: Science and Systems Foundation, Jun 2019.

[13] W. Ding, *Self-Excited Vibration: Theory, Paradigms, and Research Methods*. Springer Berlin Heidelberg, 2010.

[14] A. Malas, and S. Chatterjee, "Generating self-excited oscillation in a class of mechanical systems by relay-feedback," *Nonlinear Dynamics*, vol. 76, no. 2, p. 1253–1269, 2014.

[15] P. Donner and M. Buss, "Cooperative swinging of complex pendulum-like objects: experimental evaluation," *IEEE Transactions on Robotics*, vol. 32, no. 3, pp. 744–753, 2016.

[16] S. S. Saidin, A. Jamadin, S. Abdul Kudus, *et al.*, "An overview: The application of vibration-based techniques in bridge structural health monitoring," *International Journal of Concrete Structures and Materials*, vol. 16, no. 1, p. 69, 2022.

[17] R. Roy, "Averaging method for strongly non-linear oscillators with periodic excitations," *International Journal of Non-Linear Mechanics*, vol. 29, no. 5, pp. 737–753, 1994.

[18] H. Lindström, P. Harris, and R. Nakada, "Methods for measuring stiffness of young trees," *Holz als Roh-und Werkstoff*, vol. 60, pp. 165–174, 2002.

[19] C. Geckeler, E. Aucone, Y. Schnider, *et al.*, "Learning occluded branch depth maps in forest environments using rgb-d images," *IEEE Robotics and Automation Letters*, vol. 9, no. 3, pp. 2439–2446, 2024.

[20] A. Gongal, S. Amatya, M. Karkee, *et al.*, "Sensors and systems for fruit detection and localization: A review," *Computers and Electronics in Agriculture*, vol. 116, pp. 8–19, 2015.

[21] B. Bartolucci, A. Rosa, C. Bertolin, *et al.*, "Mechanical properties of the most common european woods: a literature review," *Frattura ed Integrità Strutturale*, vol. 14, pp. 249–274, 08 2020.